



Rapid and sensitive detection of glucocorticoids using engineered magnetosomes functionalized protein A conjugated broad-spectrum monoclonal antibody

Jinxin He^{a,*}, Yuan Wang^a, Yaqing Hou^a, Fang Tang^a, Jiesheng Tian^{b,*}

^a College of Veterinary Medicine, Shanxi Agricultural University, Taigu, Shanxi 030801, PR China.

^b State Key Laboratory of Agrobiotechnology, College of Biological Sciences, China Agricultural University, Beijing 100193, China.

ARTICLE INFO

Keywords:

Engineered Magnetosome
Protein A
Broad-spectrum monoclonal antibody
Immunomagnetic assay
Glucocorticoids

ABSTRACT

Engineered bacterial magnetic nanoparticles (BMPs) fused with protein A (BMP-PA) can bind antibodies, creating immunomagnetic beads that offer an attractive tool for targets screening. In the study, BMP-PA-IgG was formed by attaching broad-spectrum monoclonal antibodies against glucocorticoids (GCs) to BMP-PA. Immunomagnetic assay was developed for analysis of GCs, using the BMP-PA-IgG and hydrocortisone-horseradish peroxidase. The developed assay exhibited broad specificity for GCs, including hydrocortisone (HCS), betamethasone (BMS), dexamethasone (DMS), prednisolone (PNS), beclomethasone (BCMS), cortisone (CS), 6- α -methylprednisone (6- α -MPNS), and fludrocortisone acetate (HFCS), with half inhibitory concentrations (IC₅₀) ranging from 0.88 to 6.57 ng/mL. The proposed assay showed average recoveries of HCS and DMS ranging from 75.6% to 105.2% in chicken and pork samples, which were correlated well with those obtained by LC-MS/MS. This study indicated that the integration of engineered immunomagnetic beads into immunoassay systems offer possibilities for the sensitive and selective detection of GCs.

1. Introduction

Immunomagnetic beads have been emerged as powerful tools in biotechnology, which have been widely used for development of various biosensor in the fields of biomedical diagnostic, environmental monitoring, and food safety (He et al., 2018,2020,2024; Edwards et al., 2019; Lewis et al., 2023). Immunomagnetic beads are typically composed of a magnetic core, spacer layer, and functionalized surface coating. The magnetic core is commonly made of iron oxide nanoparticles with excellent magnetism and biocompatibility, and spacer layer acts as a protective barrier, preventing direct interaction between magnetic core and functionalized surface. Antibodies are usually coated on the functionalized surface, which confer specificity for targets. Thus, the key function of immunomagnetic beads is the selective binding and separation of target molecules using external magnetic fields (Wang & Lin, 2018). When in contact with targets, antibodies on surface bind specifically to them, allowing for their extraction from complex samples (He et al., 2018,2020). In addition, the targeted isolation enables the enrichment of rare targets in samples, thereby enhancing sensitivity and accuracy in diagnostics (Chen et al., 2016).

By harnessing their unique composition, function, and magnetic properties, immunomagnetic beads offer unprecedented benefits for separation and analysis of targets (Hong et al., 2023; Tao et al., 2023). Therefore, the future of immunomagnetic bead technology holds tremendous promise for further advancement in multiple domains. However, most of functionalized magnetic beads in use are chemically synthesized, which may undergo aggregation or agglomeration, thereby affecting their performance and consistency in applications (Ali et al., 2016). Moreover, some chemically synthesized magnetic beads may contain toxic substances or by-products from synthesis process through co-precipitation. Furthermore, large-scale production of chemically synthesized magnetic beads can be challenging, making it difficult to meet the growing demands of such beads (Ali et al., 2016). Consequently, there is an urgent requirement for the development of alternative immunomagnetic beads to address these concerns.

Magnetosomes (also termed bacterial magnetic nanoparticles (BMPs)) are unique biominerals produced by magnetotactic bacteria, encapsulating either magnetic (Fe₃O₄) or greigite (Fe₃S₄) within a phospholipid bilayer membrane adorned with specific proteins such as mamC and mamF (Uebe & Schüller, 2016). These particles exhibit

* Corresponding authors.

E-mail addresses: hjx@sxau.edu.cn (J. He), tianhome@cau.edu.cn (J. Tian).

<https://doi.org/10.1016/j.fochx.2024.101523>

Received 1 April 2024; Received in revised form 27 May 2024; Accepted 27 May 2024

Available online 29 May 2024

2590-1575/© 2024 The Authors. Published by Elsevier Ltd. This is an open access article under the CC BY-NC license (<http://creativecommons.org/licenses/by-nc/4.0/>).

superior characteristics compared to chemically synthesized magnetic beads, including uniform size distribution, precise crystal structure, robust thermal stability, and exceptional colloidal stability (Yan et al., 2017). Consequently, chemically functionalized BMPs have garnered significant attention across a diverse array of applications, ranging from immunoassay and biosensors to drug delivery system and biomedical imaging (He et al., 2018, 2020; Baki et al., 2021; Ren et al., 2023). While chemical modification strategies have proven effective in constructing immunomagnetic beads using BMPs, they can potentially compromise the functionality and orientation of attached molecules due to the cross-linking processes involved. This has led to increased interest in the use of genetic modification techniques, which are both cost-effective and environmentally sustainable, for the functionalization of BMPs in the context of target separation and analysis (He et al., 2018, 2020; Xu et al., 2014).

Researchers have harnessed the mamC or mamF membrane proteins of BMPs to display a variety of functional proteins on their surfaces, such as immunoglobulin G-binding domains (Yoshino & Matsunaga, 2006), thyroid-stimulating hormone receptor (Kanetsuki et al., 2012), protein G (Takahashi et al., 2009), G protein-coupled receptors (Yoshino et al., 2021), and nanobody (Wu et al., 2021). In prior research, we successfully expressed protein A (PA) on BMPs, thereby enabling it to bind to IgG and create immunomagnetic beads capable of selectively targeting gentamycin and *Vibrio parahaemolyticus* (Xu et al., 2014, 2019). However, despite these advancements, a comprehensive evaluation of the systematic application and performance of genetically engineered BMPs for the separation and analysis of trace targets in animal-derived food remains an uncharted area to date.

Glucocorticoids (GCs), a group of steroidal compounds with potent anti-inflammatory, anti-allergic, and anti-shock properties, have seen widespread usage in veterinary medicine (He et al., 2022). Despite their therapeutic benefits, the excessive or inappropriate administration of GCs can result in their accumulation within animal tissues, subsequently finding their way into the human food chain. This introduces potential health hazards, encompassing detrimental impacts on the immune system, suppression of growth hormone production, and a host of other complications (Quatrini & Ugolini, 2021). Thus, the Europe Union has established the maximum residue limits (MRLs) for dexamethasone (DMS) and betamethasone (BMS) at 0.75 µg/kg of muscle and kidney, 2.00 µg/kg of liver, and 0.30 µg/kg of milk (Council Regulation 37/2010/EC of 22 December of, 2009). In parallel, China has regulated the MRL for DMS in muscle tissue was set at 0.75 µg/kg (China, 2002).

Despite the existence of multiple methods devised to monitor GCs residues in food products, a biogenic immunomagnetic bead-based immunoassay specifically for GCs screening has yet to be documented. To address this gap, PA was genetically displayed onto BMPs to construct functional immunomagnetic beads via PA reaction with a broad-spectrum monoclonal IgG antibody targeting various GCs. The developed BMP-PA-IgG complex, when coupled with a suitable tracer, effectively integrates separation and analysis of GCs residues. The experimental outcomes demonstrated that the genetically modified BMPs, equipped with PA conjugated to a broad-spectrum monoclonal antibody, hold considerable promise for the highly sensitive and selective detection of GCs residues in food matrices. This novel approach significantly advances the field, offering a potential solution for the accurate monitoring and control of GCs contamination in the food supply chain.

2. Experimental

2.1. Chemical and materials

Hydrocortisone (HCS), dexamethasone (DMS), betamethasone (BMS), prednisolone (PNS), beclomethasone (BCMS), cortisone (CS), 6- α -methylprednisone (6- α -MPNS), and fludrocortisone acetate (HFCS) were purchased from Yuhao Chemical Technology Co. LTD (Hangzhou,

China). N-hydroxysuccinimide (NHS), Dimethyl formamide (DMF), 1-ethyl-3-(3-dimethylaminopropyl) carbodiimide hydrochloride (EDC), isopropyl β -D-thiogalactopyranoside (IPTG), 3,3',5,5'-tetramethylbenzidine (TMB), and horseradish peroxidase (HRP) were obtained from Sigma-Aldrich (St. Louis, MO, USA). 96-well plates were procured from Thermo Fisher Scientific Inc. (Rockford, IL). N, N-Dimethylformamide (DMF) and methanol were obtained from Sinopharm Chemical Reagent (Shanghai, China).

2.2. Fusion expression of PA on BMPs

The recombinant strain *M. gryphiswaldense*, carrying the pBBR-mamF-PA plasmid, was activated and transformed into a 42-L fermentation medium using our previously established methods (Xu et al., 2014, 2019). The composition of fermentation medium and feeding media was performed based on the findings of previous study (Zhang et al., 2011). After 12 h of cultivation, 7.5 mL of 1 M IPTG was added to initiate the expression of mamF-PA gene. Following an additional 30 h of growth, the bacterial pellet was harvested and suspended in PBS (0.01 M, pH 7.4). Cell disruption was achieved using ultrasonication (80 W), which were repeatedly for several times until the protein concentration in the supernatant no further decreased. Then, western blotting analysis was performed to verify the PA displayed on BMPs, adopting a minor adaptation from our preceding studies (He et al., 2018, 2020; Xu et al., 2019). The membrane proteins of BMPs and BMP-PA were separated by sodium dodecyl sulfate polyacrylamide gel electrophoresis (SDS-PAGE), and the bands were transferred onto a nitrocellulose membrane. To curtail nonspecific binding, the membrane was incubated with 1% BSA at 4 °C overnight. Subsequently, the rabbit serum IgG against PA (1:4000) was incubated with the membrane under gentle agitation for 1 h at room temperature. Afterward, the membrane underwent rigorous washing to discard any unbound primary antibodies. A goat anti-rabbit IgG secondary antibody, conjugated to HRP, was then applied to membrane for another hour. Afterward, the membrane was washed three times with tris-buffered saline with Tween-20 (0.05%), the reactivity was detected using an enhanced chemiluminescence solution.

To visualize the morphology of purified BMP-PA, a 10 µL suspension was air-dried on copper mesh and examined using transmission electron microscopy (TEM). The hydrated radii and zeta potential of the BMP-PA were measured using Zeta-PALS. Finally, the purified BMP-PA was washed twice with distilled water under ultrasonication, captured using a magnet, and stored at 4 °C for further study.

2.3. Synthesize HCS tracer

To synthesize HCS tracer, a carboxyl group was introduced into the HCS molecule using a previously described method (He et al., 2022). The HCS (500 mg) was weighted into a round-bottomed flask with addition of 5 mL of pyridine. Then, succinic anhydride (110 mg) was added to the solution, and the mixture was stirred continuously at 80 °C for 3 h. After the reaction, vacuum distillation was carried out to collect residue, which was then resuspended in 10 mL of ice water. Then, white crystalline solids were gradually formed in the solution. These solids were subsequently precipitated from the solution, filtered, and dried, resulting in the formation of HCS derivatives with a carboxyl group (HCS-COOH). Next, HCS-COOH was conjugated to HRP to produce the HCS tracer. This conjugation process followed the methodology described in our previous reports (He et al., 2018, 2021).

2.4. BMP-PA-IgG based ELISA for HCS

The 1 mg of BMP-PA (in 0.5 mL) was combined with 2 mg/L IgG solution and incubated at 37 °C for an hour. This step facilitated the conjugation between BMP-PA and IgG. Subsequently, to purify the complex, the BMP-PA-IgG mixture was subjected to a washing process

three times using PBST in a 96-well magnetic plate, which aided in removing any unbound or non-specifically bound molecules. To prevent non-specific binding in subsequent assay steps, the washed BMP-PA-IgG complexes were then blocked overnight at 4 °C with 1% gelatin solution.

To construct immunomagnetic bead-based ELISA, the concentration of BMP-PA-IgG and HCS-HRP tracer was determined by checkboard method. The experiment was conducted using 96-well plates, which were initially blocked with 1% gelatin (300 μ L per well) in carbonate-bicarbonate buffer (pH 9.6) and left to incubate at 4 °C overnight. Following the incubation, the plates were washed with PBST (PBS, 0.01 M, pH 7.4, containing 0.5% tween-20). BMP-PA-IgG complexes were also blocked with 1% gelatin overnight. Subsequently, the BMP-PA-IgG suspension was added to the plates (100 μ L per well) and then washed three times with PBST in 96-well magnetic frame. Next, a series of dilution of HCS solutions (50 μ L) were added to the respective wells, respectively. Subsequently, HCS tracer (50 μ L) was also added to each well. The mixture was incubated on an oscillator (150 rpm/min) for 10 min without a magnet. Following washing three times with PBST, TMB solution (100 μ L) was added to each plate. The TMB solution was prepared by diluting 400 μ L of 0.6% TMB and 100 μ L of a 1% H₂O₂ solution in 25 mL of citrate buffer with a pH of 5.5. The reaction was allowed to proceed for 10 min, and it was then stopped by adding 50 μ L of 2 M H₂SO₄. The absorbance of the plates was measured at 450 nm using a microtiter plate reader. To determine the assay sensitivity, the half-maximum signal inhibition concentration (IC₅₀) was calculated using a four-parameter logistic equation generated by SigmaPlot10. Additionally, the limit of detection (LOD, represented as IC₁₀), was also determined using the same equation.

To investigate the impact of physicochemical parameters on performance indicators, namely the maximal signal (A₀) and IC₅₀ of BMP-PA-IgG ELISA, a series of experiments were designed. These experiments spanned a broad spectrum of pH values (4.0 to 10.0), methanol concentrations (0% to 40% v/v), and sodium chloride concentrations (0 to 1.094 M). A distinctive exception to this systematic variation was observed in one particular experimental condition, which consisted of a pH of 8, 0.137 M NaCl, 0.003 M KCl, and 10% methanol. This unique combination of variables served as a point of contrast, enriching the overall assessment by providing insights into the ELISA's behavior under distinct physicochemical conditions.

2.5. Cross reactivity of BMP-PA-IgG based ELISA

To determine the specificity of the BMP-PA-IgG-based ELISA, the IC₅₀ values of HCS were compared with those of various chemical compounds, such as DMS, BMS, PNS, BCMS, CS, 6- α -MPNS, and HFCS by the immunomagnetic assay, respectively. Then, cross reactivity (CR) was calculated using the following equation: CR (%) = [IC₅₀ (HCS)/IC₅₀ (tested compound)] \times 100%.

2.6. Sample pretreatment

Pork and chicken muscle samples were obtained from local market (Taigu district, China) for recovery study. Prior to analysis, the samples were tested for the absence of GCs by liquid chromatography-tandem mass spectrometry (LC-MS/MS) according to a previous report (He et al., 2022). Subsequently, the chicken and pork samples (2 g each) were weighted and placed in separate 50-mL glass tubes for homogenization, respectively. The samples were spiked with HCS and DMS (with a stock solution in DMF at 100 ng/mL) at the concentration of 2, 10, and 50 μ g/kg. The extraction process involved two cycles of ultrasonic bath treatment with 10 mL of methanol for 30 min each. The resulting upper liquids were collected by centrifugation at 4000 g for 10 min. The combined methanol extract was then evaporated to dryness in a water bath at 56 °C. The residue was redissolved in 200 μ L methanol and then diluted 5-fold, 10-fold, and 20-fold with PBS (pH 8, containing 10% methanol) to mitigate matrix effects and facilitate the detection of

low levels of GCs, respectively, before performing the BMP-PA-IgG-based ELISA. These tissue extracts were analyzed using the LC-MS/MS techniques (He et al., 2022), exhibiting robust linearity for the detection of GCs in both chicken and pork muscle samples across a wide concentration spectrum of 0.8 to 100 ng/mL ($r^2 = 0.9993$). The LOD was set at 0.5 ng/mL. The recoveries for GCs ranged from 85.16% to 110.42%, with relative standard deviations (RSDs) of <11.46%. Furthermore, matrix effects were found to be <23%, thus validating the effectiveness of the applied analytical approach.

3. Results and discussion

3.1. Purification of BMP-PA

The synthesis of BMPs involves the cultivation of magnetotactic bacteria under specific conditions, allowing them to synthesize intracellular magnetic nanoparticles. BMPs can be obtained by fermentation MTB, which has been successfully scaled up to a 42-L fermentor (He et al., 2020; Liu et al., 2010). After genetic manipulation, these nanoparticles are purified and coated with specific decoration on the surface of the BMPs (Wu et al., 2021; Xu et al., 2014, 2019). Among the BMP-associated proteins in MSR-1, mamF is considered the most stable and commonly used in BMP surface display systems (Grünberg et al., 2004). In our previous study, the chromosomal mamF gene was deleted, and fusion gene mamF-PA was expressed in recombinant plasmid pBBR-mamF-PA (Xu et al., 2014, 2019). In this study, MTB containing pBBR-mamF-PA plasmid were cultured in a 42-L fermentor to produce the BMP-PA. After 36 h of culturing, the cells were harvested with a weight reaching 2.53 g/L. BMP-PA was further purified through ultrasonication with a yield of 60.78 mg/L, which was consistent with our previous study (Xu et al., 2014, 2019). To verify the presence of PA on the surface of BMP, western blotting was performed with an expected bands around 55 kDa (Fig. 1), which was in line with our expectation (Xu et al., 2014). These findings indicate that BMP-PA is potentially useful for industrial fermentation processes.

3.2. Characteristics of engineered BMP-PA and BMP-PA-IgG

The PA displayed on BMPs could interact with Fc domain of antibodies, leading to the formation of BMP-PA-IgG complexes (Ma et al., 2022; Xu et al., 2019). To create a novel immunomagnetic bead targeting GCs, a broad-spectrum monoclonal antibody that specifically

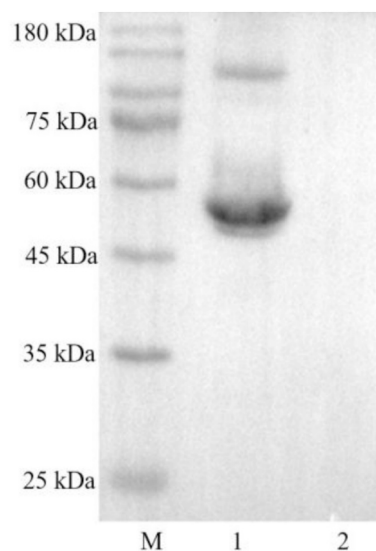


Fig. 1. Identification of PA expressed on BMPs by western blotting. Line M, protein marker; Line 1, BMP-PA; Line 2, wild-type BMPs.

binds to GCs was incorporated with BMP-PA. The properties of BMP-PA and BMP-PA-IgG were subsequently evaluated. The sizes distribution of BMPs, BMP-PA, and BMP-PA-IgG ranged from 20 to 70 nm in diameter, as observed by TEM image (Fig. 2 and Fig. S1). In a stable water-based suspension system, the zeta potential, which reflects the surface charge of dispersed particles, ideally should be above +30 mV or below -30 mV. The low zeta potentials of BMP-PA and BMP-PA-IgG nanoparticles were found to be -48.68 mV and -43.25 mV (Table S1), indicating excellent stability of the colloidal suspension in water. The average hydrated radius was measured to be 263.5 nm for BMPs, 281.2 nm for BMP-PA, and 313.3 nm for BMP-PA-IgG (Table S1). To evaluate the function of BMP-PA-IgG for targeting GCs, a tracer needed to be synthesized. The IgG against GCs had shown a proper affinity to HCS in previous study (He et al., 2022). Thus, carboxyl group was introduced to HCS as confirmed by LC-MS analysis (Fig. S2), and it was conjugated with HRP to serve as the tracer (Fig. S3) ($p < 0.01$). Their unique attributes make them exceptionally suitable for immunomagnetic assay.

3.3. BMP-PA-IgG based ELISA for GCs

Immunomagnetic assays have revolutionized the detection and measurement of trace small molecules due to their superior sensitivity, specificity, and efficiency (He et al., 2018, 2020, 2024; Xu et al., 2019). However, the non-covalent binding of PA to the Fc region of antibodies in BMP-PA-IgG assay can be influenced by several factors such as pH, ionic strength, and the presence of organic solvents like methanol. In this investigation, the performance of the BMP-PA-IgG based ELISA under various challenging conditions was meticulously assessed. The assay was carried out with BMP-PA-IgG incubated in solutions having a broad spectrum of pH levels (from 4 to 10), NaCl concentrations (from 0 to 1.094 M), and methanol percentages (0 to 40%). Notably, the results revealed that the assay displayed optimal sensitivity at a basic pH of 8, registering the lowest IC_{50} value of 0.98 ng/mL (Fig. 3A), possibly due to enhanced BMP-PA-IgG stability and improved HCS solubility under these conditions (He et al., 2022). Consequently, PBS buffered at pH 8 was chosen for subsequent experiments. While anti-GCs IgG has

previously demonstrated resilience against methanol (He et al., 2024), the effect of this organic solvent on the BMP-PA-IgG-based ELISA required evaluation before its application in incurred samples. Fig. 3B shows that as methanol concentration increased from 0 to 40%, the IC_{50} values fluctuated between 0.94 and 1.31 ng/mL and A0 readings ranged from 0.715 to 1.068. Remarkably, at a 10% methanol concentration, the assay achieved its highest sensitivity ($IC_{50} = 0.94$ ng/mL) along with a suitable A0 reading of 1.015, indicating that methanol at this level stabilizes HCS for use in the BMP-PA-IgG competitive ELISA without significantly affecting the binding affinity. Regarding NaCl concentration, increasing it from 0 to 1.094 mol/L led to variations in IC_{50} values from 0.91 to 1.91 ng/mL and A0 values from 0.725 to 1.061 (Fig. 3C). The elevated ionic strength seemed to disrupt the interaction between the antibody and analyte, thereby reducing the assay's signal intensity and sensitivity. Under the tested conditions, an ionic strength of 0.137 mol/L NaCl in PBS (pH 8 and 10% methanol) provided the best compromise with a commendable A0 of 1.061 and a relatively low IC_{50} of 0.91 ng/mL, hence making it the preferred choice for the ongoing study.

Under optimal conditions, the competitive inhibition curve for HCS was constructed (Fig. 4). The IC_{50} value, limit of detection (LOD) at 10% inhibition, and linear range (IC_{20} - IC_{80}) for HCS were determined to be 0.91 ng/mL, 0.03 ng/mL, and 0.11 to 6.78 ng/mL, respectively. BMPs possess a large surface area and high antibody loading capacity, which enhances target capture efficiency (Xu et al., 2019). This leads to increased sensitivity and lower detection limits, enabling accurate quantification of GCs even at low concentration ranges. Additionally, the LODs for DMS, BMS, PNS, BCMS, CS, 6- α -MNPS, and FHCS were found to be 0.02, 0.08, 0.09, 0.04, 0.11, 0.21, and 0.19 ng/mL, respectively (Table 1). These LODs meet the MRLs for GCs in chicken and pork samples set by the Europe and China, making this method suitable for monitoring GCs residual levels in practical applications. To assess the specificity of the method, the inhibition curves were tested to calculate the CR values for GCs. The results demonstrated various CR values (ranging from 13.85% to 103.4%) for the GCs using BMP-PA-IgG, of which the IC_{50} value for DMS in the assay was 0.88 ng/mL (Table 1). This suggested that the antibody had a higher affinity for DMS compared

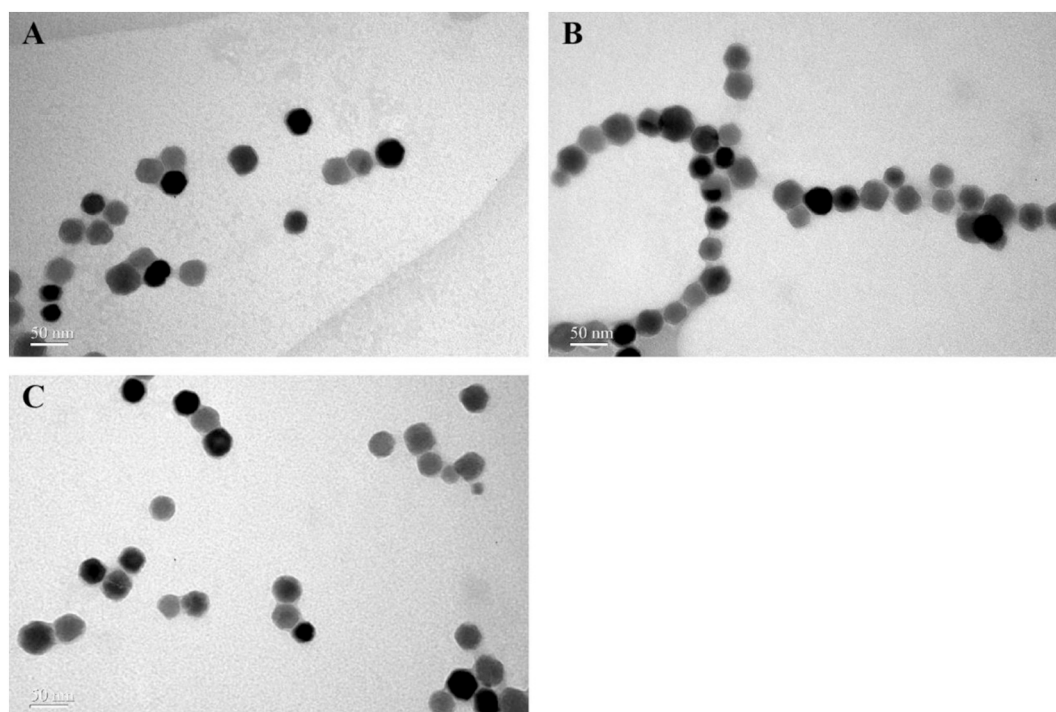


Fig. 2. Morphology and particle size of immunomagnetic beads. TEM image of particles BMPs (A), BMP-PA (B), and BMP-PA-IgG (C).

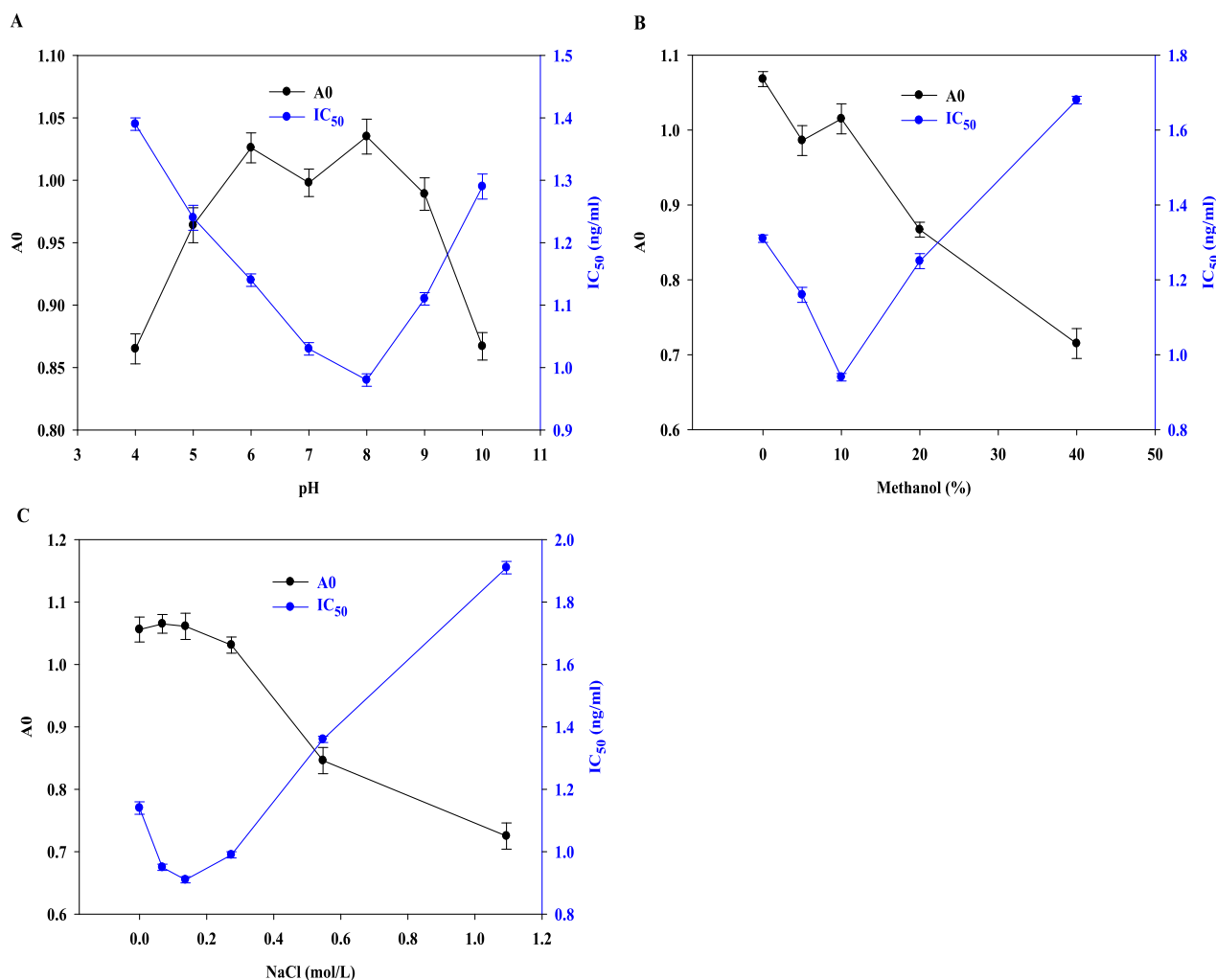


Fig. 3. Effects of pH (A), methanol (B), and NaCl (C) on the performance of BMP-PA-IgG based immunomagnetic assay for GCs. The data shown were the average of triplicates.

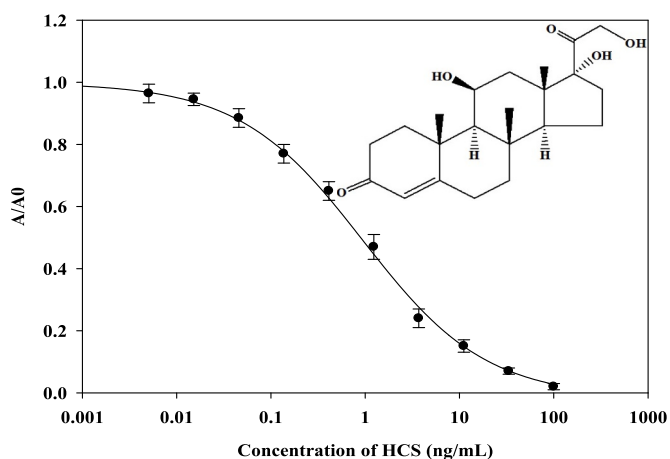


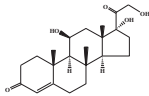
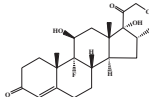
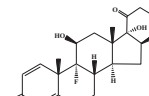
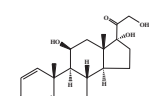
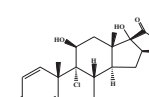
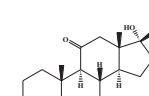
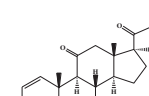
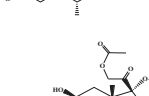
Fig. 4. Calibration curve of BMP-PA-IgG-based ELISA for HCS. The data shown are the average of triplicates.

to HCS (He et al., 2022). These findings suggested combination of BMP-PA-IgG with immunoassay platforms brings several advantages such as high-throughput capability, swift assay time, and simplified operation to the GCs detection process.

3.4. Analysis of GCs in samples

Immunomagnetic beads enable easy and efficient separation using a magnetic field, making them well-suited for immunoassay applications. However, the presence of matrix effects in samples is unavoidable and can lead to misinterpretation of results in immunoassays (He et al., 2018, 2020, 2021). While immunomagnetic beads facilitate the separation of targets from samples, it is crucial to consider the matrix effect resulting from the reaction between the antibody and targets. Dilution of the extracts can help mitigate the matrix effects. For detection of GCs in chicken and pork samples using BMP-PA-IgG, a ten-fold dilution with PBS (0.01 M, pH 8) containing 10% methanol was found to remove the matrix effects (Fig. S4). Subsequently, spiking and recovery tests were performed to detect low levels of HCS and DMS (Table 2). Although the BMP-PA-IgG exhibited high tolerance to methanol, the samples extracts were uniformly dissolved in 10% methanol. The chicken and pork samples were spiked with low, medium, and high concentrations of HCS and DMS measured by the BMP-PA-IgG based ELISA. The average recoveries of the three spiked concentrations for HCS and DMS ranged from 75.6 to 105.2%, with variable coefficient (CV) <9% (Table 2). This assay was also applied to detect GCs residues in real samples collected from Taigu area, having GCs levels in a range of <LOD–2.54 ng/g and < LOD–1.96 ng/g (Table S2), indicating the method had high accuracy and precision when applied to chicken and pork samples. The results of ELISA and LC-MS/MS showed good correlations (Fig. S5). The

Table 1
Parameters of BMP-PA-IgG based ELISA for GCs.

Analytes	Structures	IC ₁₀ (ng/mL)	IC ₅₀ (ng/mL)	CR (%)	MRLs in muscle (μg/kg)	
					China	EU
HCS		0.03	0.91	100	–	–
DMS		0.02	0.88	103.4	0.75	0.75
BMS		0.08	1.57	57.96	0.75	0.75
PNS		0.09	3.65	24.93	4	4
BCMS		0.04	1.36	66.91	4	4
CS		0.11	5.67	16.05	–	–
6-α-MPNS		0.21	6.57	13.85	10	10
HFCS		0.19	4.41	20.63	–	–

Note: –, no MRLs.

Table 2
Determination of DMS and HCS in chicken and pork samples by BMP-PA-IgG based ELISA and LC-MS/MS.

Samples	Analytes	Spiked level (ng/mL)	Average recovery (%) ± CV (n = 3)	
			ELISA	LC-MS/MS
Chicken	DMS	0	0	0
		2	87.6 ± 1.42	92.1 ± 1.34
		10	90.2 ± 4.26	93.2 ± 2.57
	HCS	50	105.2 ± 5.16	96.5 ± 4.35
		0	0	0
		2	82.6 ± 1.28	97.2 ± 1.32
Pork	DMS	10	93.6 ± 4.17	101.3 ± 3.54
		50	104.7 ± 6.37	97.3 ± 3.58
		0	0	0
	HCS	2	75.6 ± 1.85	87.6 ± 1.59
		10	86.4 ± 3.67	96.7 ± 3.54
		50	92.4 ± 8.35	95.6 ± 5.24
		0	0	0
		2	79.5 ± 1.17	89.7 ± 1.54
		10	90.4 ± 4.68	92.6 ± 4.52
50	92.1 ± 6.57	95.2 ± 3.53		

results indicated that BMP-PA-IgG based assay was accurate and could be used for the high-throughput screening of GCs in real samples.

4. Conclusions

This study utilizes engineered BMPs fused with PA (BMP-PA), which effectively binds a monoclonal antibody specific to GCs, thereby producing immunomagnetic beads that are highly efficient for target analyte capture. A key aspect of the methodology involves the derivatization of HCS and its subsequent conjugation to HRP, serving as a sensitive tracer in the assay. Building upon this, an immunomagnetic bead-based assay was devised, leveraging the BMP-PA-IgG complex alongside the HCS-HRP tracer. This novel immunomagnetic approach was successfully implemented for the quantification of GCs in both chicken and pork samples, demonstrating notable sensitivity and accuracy in recovery tests. Importantly, the results correlated excellently with those obtained from LC-MS/MS method, validating the reliability of the proposed assay. In summary, the immunomagnetic assay presented herein exhibits great potential as a rapid, high-throughput screening tool for the detection of GCs residue levels, offering a practical and efficient alternative for monitoring purposes in food safety applications.

CRedit authorship contribution statement

Jinxin He: Writing – review & editing, Methodology, Conceptualization. **Yuan Wang:** Resources, Formal analysis, Data curation. **Yaqing Hou:** Validation, Software, Methodology. **Fang Tang:** Investigation, Data curation. **Jiesheng Tian:** Writing – review & editing, Visualization, Supervision.

Declaration of competing interest

The authors declare that they have no known competing financial interests or personal relationships that could have appeared to influence the work reported in this paper.

Data availability.

Data will be made available on request.

Data availability

Data will be made available on request.

Acknowledgments

This work was supported by the National Key Research and Development Program of China (2023YFD1301501), Project of Science and Technology Innovation and Promotion of Shanxi Agricultural Universities (CXGC2023022), Shanxi Province Science Foundation for Youths (20210302124139).

Appendix A. Supplementary data

Supplementary data to this article can be found online at <https://doi.org/10.1016/j.fochx.2024.101523>.

References

- Ali, A., Zafar, H., Zia, M. U., Haq, I., Phull, A. R., Ali, J., & S., & Hussain, A.. (2016). Synthesis, characterization, applications, and challenges of iron oxide nanoparticles. *Nanotechnology, Science and Applications*, 9, 49–67. <https://doi.org/10.2147/NSA.S99986>
- Baki, A., Wiekhorst, F., & Bleul, R. (2021). Advances in magnetic nanoparticles engineering for biomedical applications-a review. *Bioengineering (Basel)*, 8, 134. <https://doi.org/10.3390/bioengineering8100134>
- Chen, Y., Xianyu, Y., Sun, J., Niu, Y., Wang, Y., & Jiang, X. (2016). One-step detection of pathogens and cancer biomarkers by the naked eye based on aggregation of immunomagnetic beads. *Nanoscale*, 8(2), 1100–1107. <https://doi.org/10.1039/C5NR07044A>
- China. (2002). No. 235 announcement on maximum residue limit for veterinary drugs in animal foods. Ministry of Agriculture and Rural Affairs of the People's Republic of China. <http://www.msybeijing.com>.
- Council Regulation 37/2010/EC of 22 December of 2009 on pharmacologically active substances and their classification regarding maximum residues limits in foodstuffs of animal origin, Brussels, Belgium. Official Journal of the European Union, L15. [http://data.europa.eu/eli/reg/2010/37\(1\)/oj](http://data.europa.eu/eli/reg/2010/37(1)/oj).
- Edwards, K. A., Randall, E. A., Tu-Maung, N., Sannino, D. R., Feder, S., Angert, E. R., & Kraft, C. E. (2019). Periplasmic binding protein-based magnetic isolation and detection of thiamine in complex biological matrices. *Talanta*, 205, Article 120168. <https://doi.org/10.1016/j.talanta.2019.120168>
- Grünberg, K., Müller, E. C., Otto, A., Reszka, R., Linder, D., Kube, M., Reinhardt, R., & Schüler, D. (2004). Biochemical and proteomic analysis of the magnetosome membrane in *Magnetospirillum gryphiswaldense*. *Applied and Environmental Microbiology*, 70(2), 1040–1050. <https://doi.org/10.1128/AEM.70.2.1040-1050.2004>
- He, J., Chen, X., Shi, S., Tang, F., Huo, N., & Gu, S. (2021). Multivalent nanobody as capture antibody-based enzyme linked immunosorbent assay for detection of 3-phenoxybenzoic acid in urine. *Analytical Biochemistry*, 632, Article 114390. <https://doi.org/10.1016/j.ab.2021.114390>
- He, J., Hou, Y., Wu, W., Li, Y., & Tang, F. (2024). Development of a broad-spectrum one-step immunoassay for detection of glucocorticoids in milk using magnetosome-based immunomagnetic beads. *Food Chemistry*, 441, Article 138377. <https://doi.org/10.1016/j.fochx.2024.138377>
- He, J., Ma, S., Wu, S., Xu, J., Tian, J., Li, J., Gee, S. J., Hammock, B. D., Li, Q. X., & Xu, T. (2020). Construction of immunomagnetic particles with high stability in stringent conditions by site-directed immobilization of multivalent nanobodies onto bacterial magnetic particles for the environmental detection of tetrabromobisphenol-A. *Analytical Chemistry*, 92(1), 1114–1121. <https://doi.org/10.1021/acs.analchem.9b04177>
- He, J., Tian, J., Xu, J., Wang, K., Li, J., Gee, S. J., Hammock, B. D., Li, Q. X., & Xu, T. (2018). Strong and oriented conjugation of nanobodies onto magnetosomes for the development of a rapid immunomagnetic assay for the environmental detection of tetrabromobisphenol-A. *Analytical and Bioanalytical Chemistry*, 410(25), 6633–6642. <https://doi.org/10.1007/s00216-018-1270-9>
- He, S., Liang, D., Xiong, J., Wang, Z., Zheng, P., Zhang, H., Ren, Z., & Jiang, H. (2022). Development of a sensitive and rapid fluorescence polarization immunoassay for high throughput screening eight glucocorticoids in beef. *Journal of Pharmaceutical and Biomedical Analysis*, 214, Article 114719. <https://doi.org/10.1016/j.jpba.2022.114719>
- Hong, B., Li, Y., Wang, W., Ma, Y., & Wang, J. (2023). Separation and colorimetric detection of *Escherichia coli* by phage tail fiber protein combined with nano-magnetic beads. *Mikrochimica Acta*, 190(6), 202. <https://doi.org/10.1007/s00604-023-05784-1>
- Kanetsuki, Y., Tanaka, M., Tanaka, T., Matsunaga, T., & Yoshino, T. (2012). Effective expression of human proteins on bacterial magnetic particles in an anchor gene deletion mutant of *Magnetospirillum magneticum* AMB-1. *Biochemical and Biophysical Research Communications*, 426(1), 7–11. <https://doi.org/10.1016/j.bbrc.2012.07.116>
- Lewis, G. L., Cernicchiaro, N., & Moxley, R. A. (2023). Effect of potassium tellurite concentration in a chromogenic agar medium on isolation of tellurite-resistant "top seven" Shiga toxin-producing *Escherichia coli* from ground beef. *Journal of Food Protection*, 86(1), Article 100017. <https://doi.org/10.1016/j.jfp.2022.11.009>
- Liu, Y., Li, G. R., Guo, F. F., Jiang, W., Li, Y., & Li, J. (2010). Large-scale production of magnetosomes by chemostat culture of *Magnetospirillum gryphiswaldense* at high cell density. *Microbial Cell Factories*, 9, 99. <https://doi.org/10.1186/1475-2859-9-99>
- Ma, S., Gu, C., Xu, J., He, J., Li, S., Zheng, H., Pang, B., Wen, Y., Fang, Q., Liu, W., & Tian, J. (2022). Strategy for avoiding protein corona inhibition of targeted drug delivery by linking recombinant affibody scaffold to magnetosomes. *International Journal of Nanomedicine*, 17, 665–680. <https://doi.org/10.2147/IJN.S338349>
- Quatrini, L., & Ugolini, S. (2021). New insights into the cell- and tissue-specificity of glucocorticoid actions. *Cellular and molecular immunology*, 18(2), 269–278. <https://doi.org/10.1038/s41423-020-00526-2>
- Ren, G., Zhou, X., Long, R., Xie, M., Kankala, R. K., Wang, S., Zhang, Y. S., & Liu, Y. (2023). Biomedical applications of magnetosomes: State of the art and perspectives. *Bioactive Materials*, 28, 27–49. <https://doi.org/10.1016/j.bioactmat.2023.04.025>
- Takahashi, M., Yoshino, T., Takeyama, H., & Matsunaga, T. (2009). Direct magnetic separation of immune cells from whole blood using bacterial magnetic particles displaying protein G. *Biotechnology Progress*, 25(1), 219–226. <https://doi.org/10.1002/btpr.101>
- Tao, T., Li, Z., Xu, S., Rehman, S. U., Chen, R., Xu, H., Xia, H., Zhang, J., Zhao, H., Wang, J., & Ma, K. (2023). Boosting SARS-CoV-2 enrichment with ultrasmall immunomagnetic beads featuring superior magnetic moment. *Analytical Chemistry*, 95(30), 11542–11549. <https://doi.org/10.1021/acs.analchem.3c02257>
- Uebe, R., & Schüler, D. (2016). Magnetosome biogenesis in magnetotactic bacteria. *Nature Reviews. Microbiology*, 14(10), 621–637. <https://doi.org/10.1038/nrmicro.2016.99>
- Wang, L., & Lin, J. (2018). Recent advances on magnetic nanobead based biosensors: From separation to detection. *TRAC, Trends in Analytical Chemistry*, 128, Article 115915. <https://doi.org/10.1016/j.trac.2020.115911>
- Wu, S., Ma, F., He, J., Li, Q. X., Hammock, B. D., Tian, J., & Xu, T. (2021). Fusion expression of nanobodies specific for the insecticide fipronil on magnetosomes in *Magnetospirillum gryphiswaldense* MSR-1. *Journal of Nanobiotechnology*, 19(1), 27. <https://doi.org/10.1186/s12951-021-00773-z>
- Xu, J., Hu, J., Liu, L., Li, L., Wang, X., Zhang, H., Jiang, W., Tian, J., Li, Y., & Li, J. (2014). Surface expression of protein A on magnetosomes and capture of pathogenic bacteria by magnetosome/antibody complexes. *Frontiers in Microbiology*, 5, 136. <https://doi.org/10.3389/fmicb.2014.00136>
- Xu, J., Liu, L., He, J., Ma, S., Li, S., Wang, Z., Xu, T., Jiang, W., Wen, Y., Li, Y., Tian, J., & Li, F. (2019). Engineered magnetosomes fused to functional molecule (protein A) provide a highly effective alternative to commercial immunomagnetic beads. *Journal of Nanobiotechnology*, 17(1), 37. <https://doi.org/10.1186/s12951-019-0469-z>
- Yan, L., Da, H., Zhang, S., López, V. M., & Wang, W. (2017). Bacterial magnetosome and its potential application. *Microbiology Research*, 203, 19–28. <https://doi.org/10.1016/j.micres.2017.06.005>
- Yoshino, T., & Matsunaga, T. (2006). Efficient and stable display of functional proteins on bacterial magnetic particles using Mms13 as a novel anchor molecule. *Applied Environmental Microbiology*, 72(16), 465–471. <https://doi.org/10.1128/AEM.72.1.465-471.2006>
- Yoshino, T., Tayama, S., Maeda, Y., Fujimoto, K., Ota, S., Waki, S., Kisailus, D., & Tanaka, T. (2021). Magnetosome membrane engineering to improve G protein-coupled receptor activities in the magnetosome display system. *Metabolic Engineering*, 67, 125–132. <https://doi.org/10.1016/j.ymben.2021.06.008>
- Zhang, Y., Zhang, X., Jiang, W., Li, Y., & Li, J. (2011). Semicontinuous culture of *Magnetospirillum gryphiswaldense* MSR-1 cells in an autofermentor by nutrient balanced and isosmotic feeding strategies. *Applied and Environmental Microbiology*, 77(17), 5851–5856. <https://doi.org/10.1128/AEM.05962-11>